Fiscal Year 2020 Filtration of Hanford Tank Waste 241-AP-105

November 2020

JR Allred
JGH Geeting
AM Westesen
EC Buck
RA Peterson

U.S. DEPARTMENT OF ENERGY

DISCLAIMER

This report was prepared as an account of work sponsored by an agency of the United States Government. Neither the United States Government nor any agency thereof, nor Battelle Memorial Institute, nor any of their employees, makes **any warranty, express or implied, or assumes any legal liability or responsibility for the accuracy, completeness, or usefulness of any information, apparatus, product, or process disclosed, or represents that its use would not infringe privately owned rights**. Reference herein to any specific commercial product, process, or service by trade name, trademark, manufacturer, or otherwise does not necessarily constitute or imply its endorsement, recommendation, or favoring by the United States Government or any agency thereof, or Battelle Memorial Institute. The views and opinions of authors expressed herein do not necessarily state or reflect those of the United States Government or any agency thereof.

Fiscal Year 2020 Filtration of Hanford Tank Waste 241-AP-105

November 2020

JR Allred
JGH Geeting
AM Westesen
EC Buck
RA Peterson

Pacific Northwest National Laboratory
Richland, Washington 99354

Summary

Bench-scale filtration testing of 11.5 liters of 241-AP-105 supernatant was conducted using a Mott inline filter Model 6610 (media grade 5) backpulsed dead-end filter (BDEF) in the hot cells of the Radiochemical Processing Laboratory at Pacific Northwest National Laboratory. The as-received samples were diluted with raw water from the Hanford Site to assess the propensity for solids to form upon dilution and to assess the impact those solids have on filtration performance.

The feed was split into two batches. The first batch was settled and decanted as planned in Tank Side Cesium Removal operations. The BDEF was used to filter this AP-105 feed at a targeted flux of 0.065 gpm/ft^2 and exhibited no measurable pressure increase during filtration.

The second batch was fed to the BDEF with solids resuspended. This was also operated at the targeted flux of 0.065 gpm/ft^2. In this case, the target pressure differential of 2 psid (resistance of 6.24×10^{10} m^{-1}) was reached in slightly more than 12 h. A backpulse restored the filter flux; however, the time to the next backpulse was slightly shorter.

These tests indicate that after the addition of raw water, settle and decant effectively removed solids from the feed. It is not possible to assess the time required for these solids to settle based on the result from these tests. However, if sufficient time is allowed for the solids to settle, no measurable filter fouling was observed in current testing. In contrast, if insufficient time is allowed for solids to settle, filter fouling will occur relatively quickly and will likely require backpulses more frequently than every 12 hours (1.91 m^3/m^2 volume filtered).

Solids concentrated from backpulse solutions displayed large variability in composition with Al-silicates and mixed chromium-aluminum oxide phases. Amounts of Mg, Fe, and Ca were also found in the presence of Na and O. These solids could be grouped in three categories: (1) soluble Na-salts that formed large block-like particles but were made up of fibrous materials, (2) amorphous Al-phases, and (3) colloidal iron oxides with an average particle diameter of 4.2 µm.

Acknowledgments

Acronyms and Abbreviations

AEA	alpha energy analysis
AOI	analyte of interest
BDEF	backpulse dead-end filter (system)
BSE	backscattered electron
CWF	clean water flux
EDS	x-ray energy dispersive spectroscopy
FEG	field emission gun
EQL	estimated quantitation limit
FIO	for information only
FY	fiscal year
GEA	gamma energy analysis
HAADF	high angle annular dark field
IC	ion chromatography
ICP-OES	inductively coupled plasma optical emission spectroscopy
IX	ion exchange
LAW	low-activity waste
MDL	method detection limit
MFC	mass flow controller
PNNL	Pacific Northwest National Laboratory
QA	quality assurance
R&D	research and development
RPL	Radiochemical Processing Laboratory
SEM	scanning electron microscopy
STEM	scanning transmission electron microscopy
TIC	total inorganic carbon
TMP	transmembrane pressure
TOC	total organic carbon
TRU	transuranic
TSCR	Tank Side Cesium Removal
WRPS	Washington River Protection Solutions
WTP	Waste Treatment and Immobilization Plant
WWFTP	WRPS Waste Form Testing Program
XRD	x-ray diffraction

Contents

Figures

Tables

1.0 Introduction

The U.S. Department of Energy's Hanford Site houses 56 million gallons of high-level radioactive waste generated from plutonium production from 1944 to 1988 (Gerber 1992). The supernatant waste, currently stored in underground tanks, is intended to be vitrified following filtration and ^{137}Cs removal at the Waste Treatment and Immobilization Plant (WTP) Pretreatment Facility. The Pretreatment Facility will not be operational for several years. The Tank Side Cesium Removal (TSCR) system is a technology demonstration that will filter and remove cesium from tank waste supernate to support directly feeding low-activity waste (LAW) to the WTP LAW Facility. The TSCR system is skid-mounted and employs two key technologies: (1) dead-end filtration for solids removal and (2) ion exchange (IX) for cesium removal. Filtration is necessary to protect the functionality of the IX columns.

A small-scale test platform to demonstrate these processes is located at the Pacific Northwest National Laboratory (PNNL) 325 Building, also known as the Radiochemical Processing Laboratory (RPL). The feed identified for the testing described herein is approximately 7.5 liters (11.5 liters after dilution) of decanted supernatant from waste tank 241-AP-105 (hereafter AP-105). This report describes the filtration process. The product from this filtration was passed on to the IX process, which is described in a following report[1].

The presence of solids has been observed in previous filtration experiments using AP-105 and AP-107 tank waste (Geeting et al. 2018a,b). The first test with AP-107 was performed with samples that were retrieved from the tank within a few weeks of raw water addition (and tank recirculation); solids were observed in those filtration experiments. Additional AP-107 samples were taken 14 months later, and filtration showed no recoverable solids (Geeting et al. 2019), indicating that settle-then-decant works to reduce solids in supernatant. Solids obtained from the first sampling event in AP-107 are suspected to be due to tank mixing and formation of precipitates when combined with process water to achieve a dilution from 8.5 to 5.6 M Na for prototypic processing conditions. Formation of solids upon dilution with process water is supported by Daniel et al. (2020), who observed that precipitates formed upon dilution of AP-105 simulant with process water. The objective of the current work was to perform filtration under prototypic conditions using Mott Grade 5 sintered metal at a targeted flux of 0.065 gpm/ft^2 planned for TSCR on two batches of diluted feed after different settling times. Filter resistance as a function of time was measured and the filter was backpulsed if the differential pressure increased to 2 psi across the filter. Backpulse solutions were collected and, if solids were found, they were analyzed.

---

[1] [Fiskum SK, AM Westesen, AM Carney, TT Trang-Le, and RA Peterson. 2020. Ion Exchange Processing of AP-105 Hanford Tank Waste through Crystalline Silicotitanate in a Staged 2- then 3-Column System. RPT-DFTP-025, Rev. 0). Pacific Northwest National Laboratory, Richland, Washington. (Currently being drafted).]

2.0   Quality Assurance

All research and development (R&D) work at PNNL is performed in accordance with PNNL's Laboratory-Level Quality Management Program, which is based on a graded application of NQA-1-2000, *Quality Assurance Requirements for Nuclear Facility Applications* (ASME 2000), to R&D activities. To ensure that all client quality assurance (QA) expectations were addressed, the QA controls of PNNL's Washington River Protection Solutions (WRPS) Waste Form Testing Program (WWFTP) QA program were also implemented for this work. The WWFTP QA program implements the requirements of NQA-1-2008, *Quality Assurance Requirements for Nuclear Facility Applications* (ASME 2008), and NQA-1a-2009*, Addenda to ASME NQA-1-2008* (ASME 2009), and consists of the WWFTP Quality Assurance Plan (QA-WWFTP-001) and associated QA-NSLW-numbered procedures that provide detailed instructions for implementing NQA-1 requirements for R&D work.

The work described in this report was assigned the technology level "Applied Research" and was planned, performed, documented, and reported in accordance with procedure QA-NSLW-1102, *Scientific Investigation for Applied Research*. All staff members contributing to the work received proper technical and QA training prior to performing quality-affecting work.

3.0 Test Conditions

In December 2019, WRPS collected 36 supernatant samples (~250 mL each) in two batches from tank AP-105 and provided them to PNNL. At its RPL facility, PNNL diluted the samples with process water (river water provided by WRPS) from 8.7 to 5.6 M Na. Dilution of the samples increased the combined volume of both batches from 7.5 liters to ~11.5 liters. Filtration testing occurred in June 2020 using a Mott Model 6610 media grade 5 in-line finger filter with porous end cap. This is a sintered 316L stainless steel filter with a 0.317-in. porous diameter, 1.463-in. porous length, and 1.51-in^2 filter area.

3.1 BDEF Dilution

The first batch of AP-105 was diluted upon receipt. Solids formation was monitored monthly to visually assess when solids formed. Four subsamples of the diluted AP-105 were centrifuged monthly to concentrate any potential solids that formed. The diluted samples were allowed to sit for 6 months prior to filtration. The decanted supernate was filtered in filter batch 1 and the bottoms of the settling containers filtered in the third filter batch. The second received batch of AP-105 was diluted in March 2020 and the samples were allowed to sit for 3 months prior to filtration. The second received batch was targeted to only sit 1 month prior to filtration; however, a shelter-in-place order in the state of Washington due to COVID-19 prohibited a filtration start date within this window. The second received batch containers were agitated to resuspend any solids before being run as filter batch 2. Figure 3.1 shows the process flow of the various aliquots for testing.
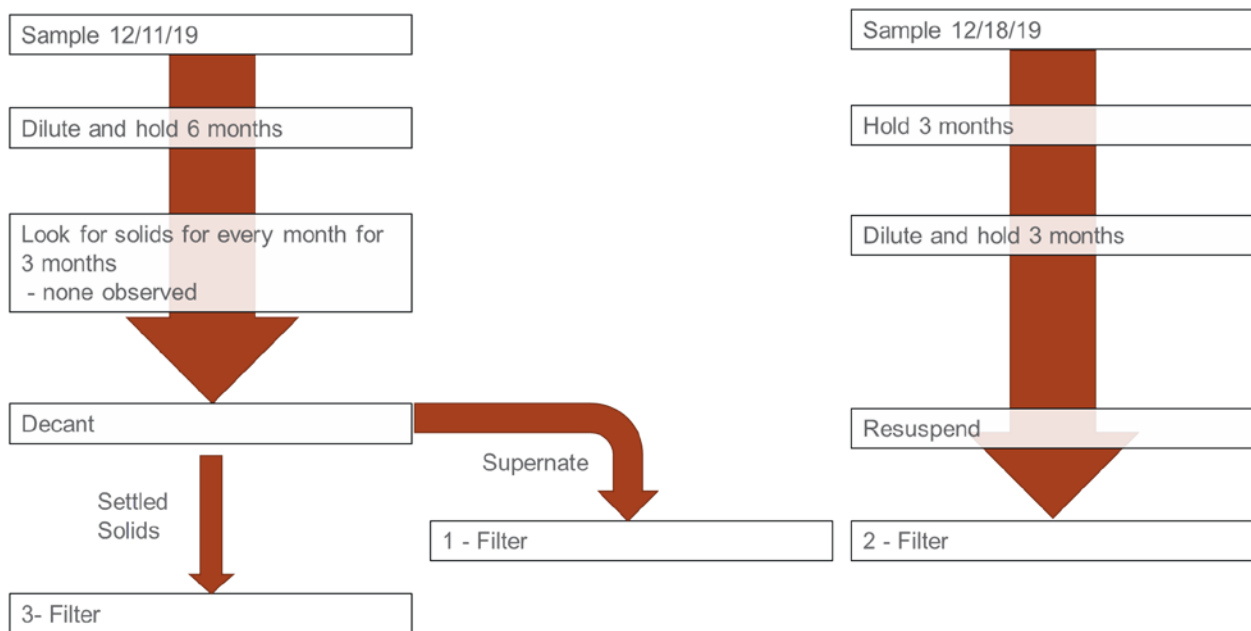
Figure 3.1. Process flow for testing

Dilution of the feed material received from tank AP-105 was based on the average measured Na concentration (8.72 M) and density (1.414 g/mL) and the target end point Na concentration (5.6 M) and density (1.250 g/mL). Dilution was performed using raw (unprocessed) river water. The mass of raw water needed to be added (m_{add}) was estimated by:

$$m_{add} = \left(\frac{c_o \, \rho_1}{c_1 \, \rho_o} - 1 \right) m_o$$

where m_o is the mass of the undiluted tank waste; c_o and c_1 are the undiluted and diluted target Na concentrations, respectively; and ρ_o and ρ_1 are the undiluted and diluted simulant densities, respectively. The dilution factor is defined as

$$DF = \frac{V_{final}}{V_{initial}}$$

where $V_{initial}$ is the initial solution volume and V_{final} is the final solution volume.

The contents of two AP-105 sample jars were combined and diluted with the process water at a mass ratio of nominally 1000:377 (tank waste: raw water) to achieve a volume dilution factor of 1.56:

$$\frac{m_{add}}{m_o} = \left(\frac{8.72 \text{ M}}{5.60 \text{ M}} \right) \left(\frac{1.250 \text{ g mL}^{-1}}{1.414 \text{ g mL}^{-1}} \right) - 1 = 0.377$$

3.2 BDEF Filtration

3.2.1 Backpulse Dead-End Filter (BDEF) System

A new filtration system to support dead-end filtration was fabricated in FY20. Functionally the system is similar to the old cell unit filter system (see Geeting et al. 2019), but smaller. This was done to reduce system internal volume and skid footprint in the hot cell to improve operational efficiency and provide flexibility to run filter tests with smaller sample volumes. A piping and instrumentation diagram is provided in Appendix A. The system is composed of a slurry recirculation loop, a filter assembly, and a permeate system. See the system installed in the hot cell below (Figure 3.2).
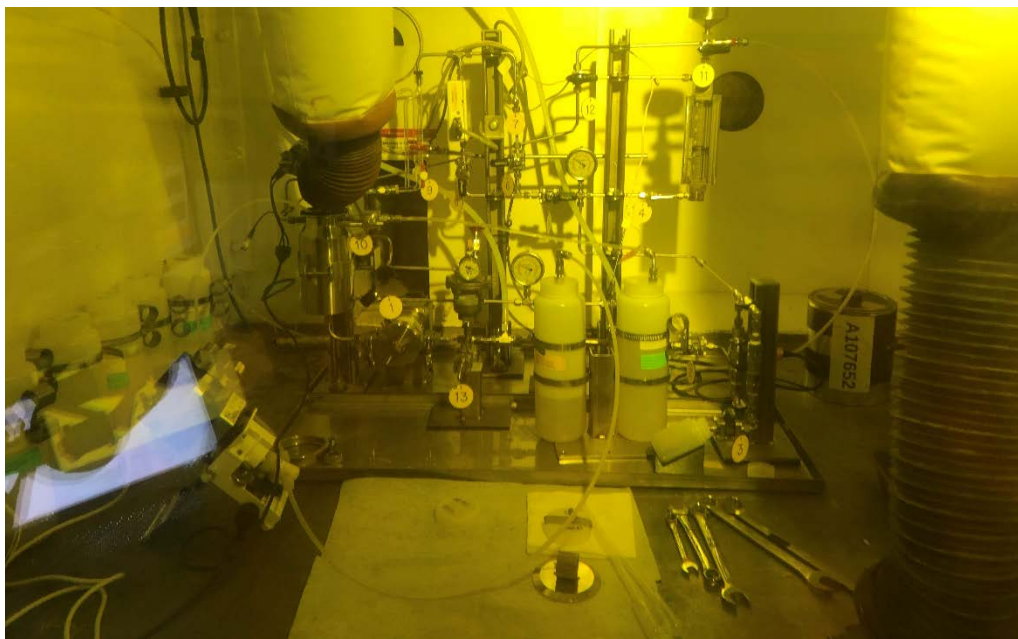
Figure 3.2. BDEF system installed in hot cell

The main recirculation loop is composed of a 1-liter stainless steel container (Eagle, EPV1A), a low-shear quaternary diaphragm pump (Quattro Flow QF150), a heat exchanger, and a throttle valve. The pump speed is controlled by a variable frequency drive that is located outside the hot cell. The slurry flow rate and pressure are controlled by adjusting the pump variable frequency drive (pump speed control) and throttle valve. The recirculation loop provides mixed, pressurized feed to the filter assembly. During the testing described in this report, the slurry temperature was maintained at 25 ± 2 °C by a chiller that circulated chilled water through an in-line shell and tube heat exchanger.

The filter assembly receives pressurized slurry from the slurry recirculation loop. The filter assembly is composed of a filter, a 0 to 2.5 psi differential pressure transducer, and a flush valve (V3 in Appendix A). The flush valve is actuated during backpulse operations used to clear solids off the filter and out of the system.

The permeate system receives permeate produced by the filter assembly. The permeate flow rate is controlled with a mass flow controller (MFC), which can control feed in the range of 0.15 to 0.33 liter/hour. (These rates equate to allowable filter areas of 1.5 to 3.3 in.^{2} assuming flux of 0.065 gpm/ft^2). The MFC measures flow rate and density of the permeate while a glass flowmeter is provided as a secondary flow rate measurement device. The permeate system can also perform a backpulse function. Pressurized air can be introduced (V12) into the backpulse chamber and used to force permeate (or other fluids) backwards through the filter and out of the system through V3.

The Mott 6610 filter used in testing is cylindrical, with dimensions of 0.317-in. diameter $\times$ 1.5-in. length and a filtration area of 1.51 in.^{2}. The filter element is fabricated from a seamless sintered stainless steel tube that is closed but porous on one end; the other end is welded to a pipe-reducing bushing. The Mott 6610 filter provided 24 hours of operation at 0.065 gpm/ft^2 with 3.7 liters of feed. Figure 3.3 shows a schematic of the filter and filter housing.

(a)

(b)

Figure 3.3. (a) Mott filter housing schematic[1] (note that the 6610 series filter was welded to a 3/8" pipe fitting, making the configuration more similar to the 6480 series) ; (b) photo of modified filters with filter housings removed

3.2.2 Backpulse Dead-End Filter System Operation

The evolutions used to test the diluted AP-105 waste samples are outlined below.

1. Clean water flux (CWF) measurement: The CWF measurement serves as a system leak test and provides a baseline measurement of the filter resistance; it was conducted at nominal test conditions (2.67 mL/min) and operated for 17 min.

2. Batch 1 – Filtered decanted AP-105 from the first batch (6-month hold time) feed with the BDEF at 2.55 mL/min: The targeted filtration rate is based on scaled flux used during AVANTech testing[2] [0.306 gpm through 4.7 ft^2 of Mott sintered metal filter (0.065 gpm/ft^2)]. The filtration rate was controlled with an MFC. Permeate was sampled near the beginning and end of Evolution 2 testing.

---

[1] Mott 6480 line filter from https://mottcorp.com

[2] *TSCR Dead End Filter Scoping Test Summary*, presentation by AVANTech Inc., November 13, 2018, Richland, Washington.

3. Batch 2 – Resuspended the solids from the second batch (3-month hold time) and filtered through BDEF at 2.55 mL/min. An increase in pressure was observed immediately after the addition of the first bottle of feed. The pressure differential steadily increased for nearly 14 hours until it reached 2 psi, when a backpulse was performed. The backpulse used a charge of 40 psi air to push nominally 26 mL [scaled from TSCR's ~77ft^2 filter area and 50 gal filter operating volume; 0.65 gal/ft^2] of filtered permeate through the filter at a rate of nominally 1.5 mL/s [scaled from 2.2 gpm/ft^2 per AVANTech communications]. After the backpulse, the pressure differential again increased, for 11 hours and 10 minutes, until it reached 2 psi again and another backpulse was performed. Filtration continued after this backpulse as normal.

4. Batch 3 – The concentrated/settled bottoms remaining after settle/decant operations supporting Batch 1 testing were combined, agitated, and then filtered at 2.55 mL/min along with the subsamples of the diluted AP-105 contained in centrifuge cones.

5. The BDEF system was drained.

6. Rinse filter: The BDEF filter was rinsed using 0.01 M NaOH.

7. CWF: After rinsing, another CWF test was planned; however, this evolution was not performed due to a failed pressure transducer.

8. The BDEF was laid-up for post-test storage.

Table 3.1 provides a mass balance for BDEF testing. A total of 14,901.35 g of AP-105 supernatant was added to the BDEF system during testing, and a total of 14,737.39 g was accounted-for. The missing mass (163.96 g) is likely due to evaporation and material that wets the inside of the BDEF system, is not recoverable, and represents approximately 1% of the initial feed.

The permeate density was measured with the Coriolis meter function of the MFC during testing and was found to be nominally 1.31 g/cm^3. This value was higher than expected and was checked gravimetrically by measuring 10 mL of each permeate collection bottle into an A grade volumetric flask and weighing on an analytical balance. These measurements resulted in a nominal value of 1.285 g/mL, which was still higher than expected.

Table 3.1. Mass balance – BDEF

Batch	Description	In (g)	Out (g)
1	Decanted supernate filtration	5742	
2	Suspended solids filtration	7565	
3	Un-decanted bottoms filtration	1594	
	Product to IX		14,328
	Permeate samples		22
	Backpulse samples		180
	Drained from BDEF		207
	Total	14901	14,737

3.3 Sample Analysis

The process water (river water) used for dilution was analyzed via:

- Inductively coupled plasma optical emission spectroscopy (ICP-OES) for the following analytes of interest (AOIs): Na, Ca, Al, B, Cr, Fe, Ni K, Si, Pb, Mo, S, and P

- Ion chromatography (IC) for the following AOIs: F, Cl, NO_3, NO_2, and SO_4

Three permeate samples (TI-094-E1-A, TI-094-E2-A, TI-094-E3-A) were collected halfway through the testing of each batch. These samples were submitted for total alpha analysis to determine the transuranic content of the filtered permeate.

A total of three backpulses were performed during filtration operations. Solutions from the backpulse containing solids were combined and equally distributed into four centrifuge tubes for solids separation. The samples were centrifuged at 2000 rpm for 5 min. The bulk amount of the supernatant was decanted and the solids from the centrifuge tubes were suspended and combined. Figure 3.4. shows the solids that were collected from the backpulsed solution after the solutions were centrifuged and decanted to further concentrate the solids. This solids slurry was split into two separate sample vials (~2 mL each) and removed from the hot cell. Both slurry samples were spun down at 3000 rpm for 2 min and the remaining supernatant was removed. The solids were washed with 10 mL of 5.6 M salt solution (1 M NaOH/4.6 M $NaNO_3$) and centrifuged again at 3000 rpm for 2 min. All liquid was decanted and the solids were left to air dry, resulting in a final dry solid mass of 0.66 gram (Note: The sample mass includes some dried salt from the 5.6 M Na solution). The dried solids were submitted for the following analyses:

- ICP-OES for the following AOIs: Na, K, Mg, Ca, Fe, Al, Si, P, S, and Cr

- Total inorganic and organic carbon (TIC/TOC)

- Optical microscopy[1]

- SEM (scanning electron microscopy) [2]

- Alpha energy analysis; AOIs: $^{239+240}$Pu, ^{238}Pu, ^{241}Am, $^{243+244}$Cm, and ^{242}Cm

- Gamma energy analysis (GEA); AOIs: ^{137}Cs, ^{60}Co, Eu isotopes, ^{241}Am, and ^{239}Pu

---

[1] See Appendix C
[2] See Appendix C
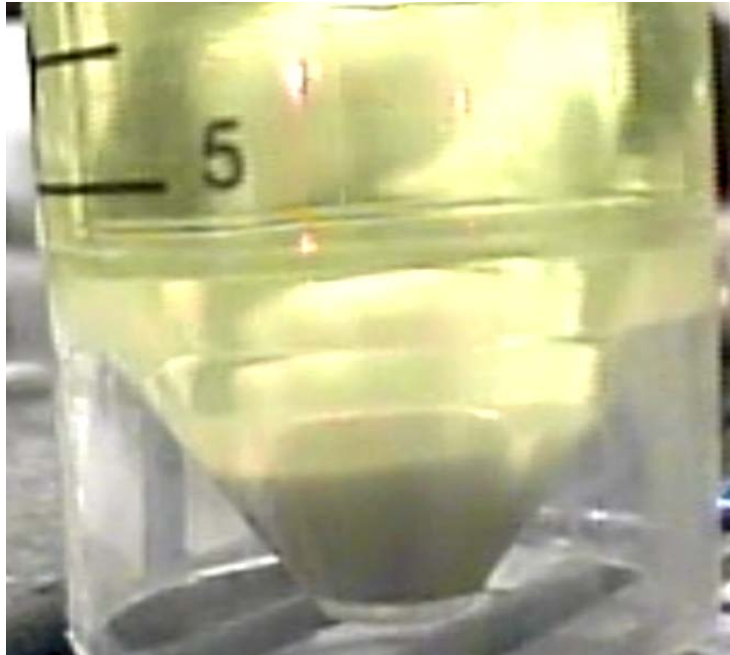
Figure 3.4. Solids backpulsed off filter, after centrifuging

4.0 Results

4.1 Dilution Process Results

Both batches of the diluted AP-105 samples were checked for density to assess the dilution. The densities were measured using 10-mL A grade volumetric flasks and an analytical balance, and ranged from 1.247 to 1.250 g/mL at an ambient cell temperature of 22.5 °C. The Na concentration was not measured after dilution but was measured after filtration (which should not affect Na concentration) and will be reported in the IX report for fiscal year (FY) 2020 (RPT-DFTP-025, *Ion Exchange Processing of AP-105 Hanford Tank Waste through Crystalline Silicotitanate in a Staged 2- then 3-Column System*; currently being drafted). Table 4.1 shows the as-received AP-105 analysis.

Table 4.1. Measured key analyte concentrations for as-received AP-105 tank waste

Analyte	As-received (M)
Na	8.72E+00
Al	7.86E-01
K	1.71E-01
Cr	9.03E-03
P	1.95E-02
S	5.27E-02

Large visible solids were observed in a few of the 250-mL receipt jars of AP-105. The as-received tank waste jars were poured through a strainer during dilution with raw water so the large solids and salt chunks would not enter the filtration system. A 0.02-g portion of these solids was collected from one of the jars and analyzed via ICP-OES; see Appendix B. The composition is summarized in Table 4.2 and an image of the solids is shown in Figure 4.1. The high iron content indicates that these solids are most likely from the carbon steel primary tank.

Prior to diluting the as-received AP-105 sample, four 30-mL aliquots were placed in centrifuge tubes and diluted in the same manner as the bulk sample. During the dilute-and-hold sequence, these aliquots were centrifuged monthly at 1500 to 3000 rpm for 5 minutes to concentrate any solids in the bottom for later measurement. No visual solids precipitation was observed. After observing for solids, these aliquots were shaken to re-homogenize the bulk fluid. This was repeated for 3 months until the COVID-19 shelter-in-place order in the state of Washington prohibited additional checks.

Table 4.2. Measured analyte composition of solids found in receipt jars

Analyte	% Composition
Fe	93.5%
Na	2.8%
Al	1.5%
Mn	0.9%
B	0.4%
Pb	0.3%
Si	0.2%
Ca	0.1%
Cr	0.1%
K	0.1%
Cu	0.04%
Ni	0.04%
Zn	0.02%
Ti	0.01%
Ba	0.01%
Cd	0.01%
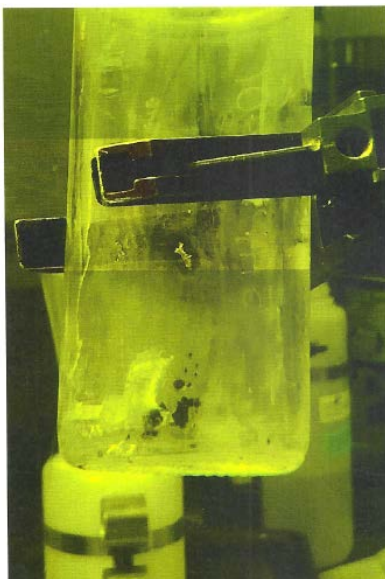
Figure 4.1. Image of solids found in receipt jar of AP-105

4.2 BDEF Filtration Results

Figure 4.2 shows the CWF, using 0.01 M NaOH, of the media grade 5 stainless steel BDEF filter before testing. The filter was also rinsed with 0.01 M NaOH just prior to the CWF test. The CWF tests were conducted at a nominal 2.55 mL/min permeate flow rate, controlled by a Brooks Quantim MFC. The transmembrane pressure (TMP) averaged 0.10 psid in the pre-CWF test. A clean flux would display a steady, not increasing differential pressure during filtration operation. No increase in differential pressure outside of system noise was seen here, giving confidence in system cleanliness. Prior (radiologically) cold testing outside of the hot cell also produced a 0.108 psid TMP average with a standard deviation of ±0.032 psid at 2.56 mL/min with deionized water.
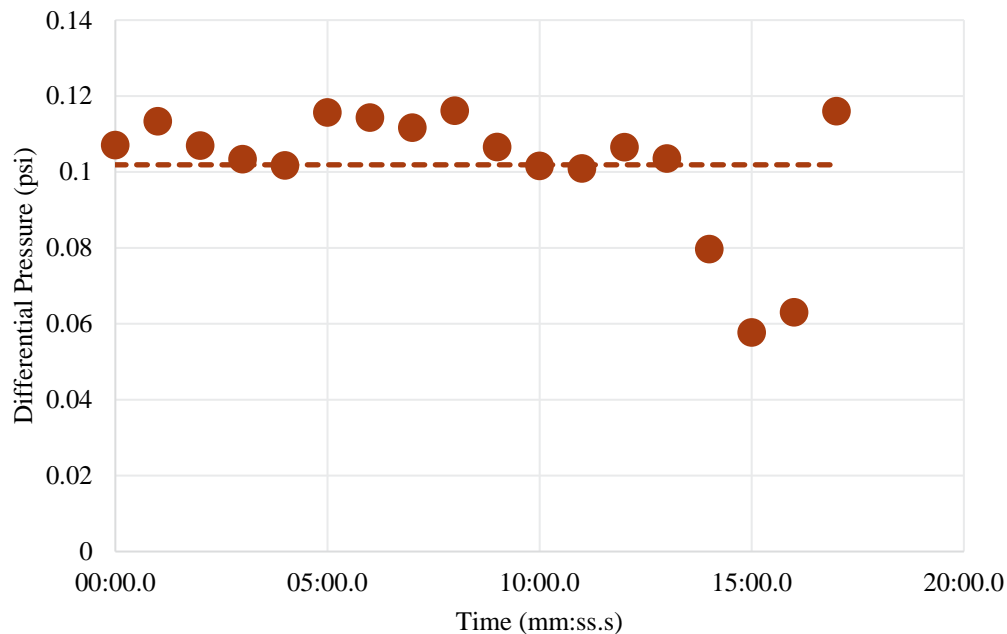
Figure 4.2. CWF measurements for media grade 5 BDEF at 0.33 liter/hour permeate rate (nominal) before testing

Figure 4.3 shows the differential pressure during the dewatering of AP-105 with the grade 5 stainless steel filter. The filtration rate was controlled via an MFC set at 2.58 mL/min (0.065 gpm/ft^2). The actual flow rate averaged 2.55 mL/min. The pressure stayed at the low end of the pressure transducer's measurement range for the first 24 h of dewatering. Line pressure was maintained at 25 to 28 psi throughout testing. As noted above (Section 3.2.2, Evolution 7), the pressure transducer was found to have failed at the completion of testing. Based on the CWF, the initial pressure drop is estimated to be around 0.58 psid following the permeability and pressure drop calculation of ISO 4022.[1] Assuming laminar flow, pressure drop across the filter increases linearly proportional to the flow rate. In this case, energy losses are due to the viscosity of the fluid only:

$$\frac{\Delta P}{e} = \alpha * \eta * \frac{Q_v}{S} = \frac{1}{P_0} * \eta * \frac{Q_s}{S}$$

---

[1] International Organization for Standardization. (2018). Permeable sintered metal materials – Determination of fluid permeability (ISO Standard No. 4022:2018).

where ΔP is the pressure drop at the filter [Pa], e is the wall thickness of the filter [m], $\alpha = \frac{1}{P_0}$ is the viscous permeability coefficient [m^{-2}], η is the dynamic viscosity of the fluid [Pa·s], Q_v is the volumetric flow rate of the fluid [m^3/s], and S is the filtration effective surface [m^2].

$$\frac{\Delta P}{e} = \alpha * \eta * \frac{Q_v}{S}$$

can be rearranged to:

$$\frac{\Delta P}{\eta} = \alpha * e * \frac{Q_v}{S}$$

Then, assuming all right-side variables remain constant between the fluid types, a viscosity ratio can be determined:

$$\frac{\Delta P_{H2O}}{\eta_{H2O}} = \frac{\Delta P_{AP-105}}{\eta_{AP-105}}$$

To determine an estimated pressure drop assuming AP-105 was at 24 °C and H$_2$O was at 22 °C:

$$\Delta P_{AP-105} = \frac{\Delta P_{H2O}}{\eta_{H2O}} * \eta_{AP-105}$$

$$\Delta P_{AP-105} = \frac{743.7 \text{ Pa}}{9.09 \times 10^{-4} \, Pa \cdot s} * 5 \times 10^{-3} \, Pa \cdot s = 0.58 \, psi$$

However, a lower pressure drop was observed: 0.2 psid. This is consistent with a clean filter and the first reading of this newly installed system. Combining uncertainties associated with viscosity, temperature, and pressure, the span between the calculated and measured pressure drops could suggest that this difference is not statistically significant when working in a hot cell environment.

The TMP of 0.2 psid was found for the first 2 hours. The initial pressure drop seen in Figure 4.3 at approximately 2 hours and the subsequent return of pressure at approximately 11 hours may have been associated with the start of the failure of the differential pressure measurement. Note that the data after 49 hours are suspect and are likely not indicative of the actual pressure drop. Following the return to anticipated TMP of 0.2 psid at 11 hours, the TMP remained there for the next 13 hours.

After 24 hours of dewatering, batch 2 was started. Immediately after introduction of batch 2, the TMP began to increase slowly and continued over the next 14 hours until it reached 2 psid. Once the backpulse criterion of 2 psid was reached, a backpulse was performed.

No visible solids were observed in the concentrate from the backpulse; however, the TMP after backpulsing was observed to drop back down to 0.2 psid (consistent with a clean filter). A second backpulse was conducted at hour 49, again with no visible solids observed in the concentrate. The TMP after the second backpulse was observed to drop down to 0.01 psid. The data after this second backpulse are suspect and are not likely indicative of actual performance. Table 4.3 summarizes the average operating parameters during each batch.
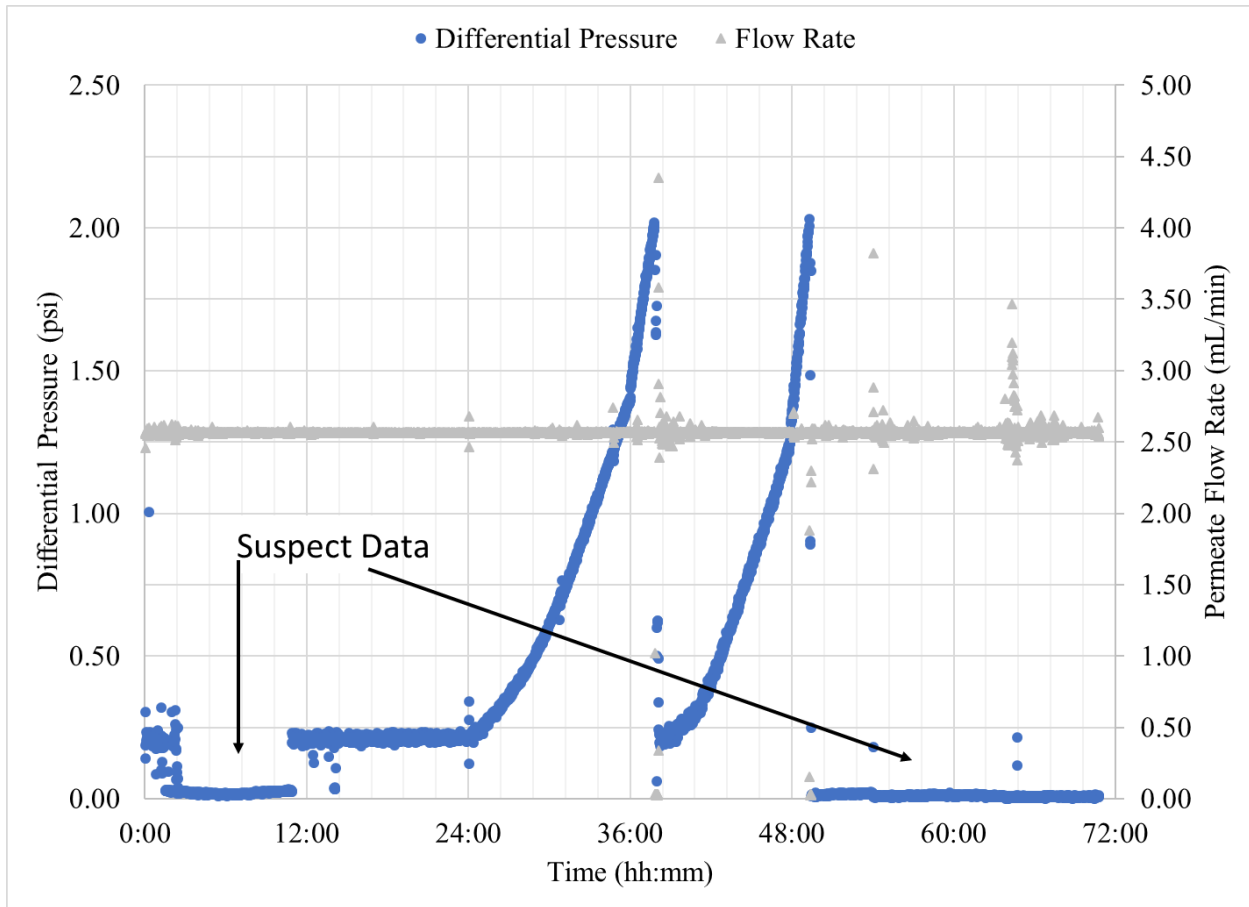
Figure 4.3. BDEF filtration evolutions 1-3

Table 4.3. Operating parameters of BDEF testing

Test Condition	Elapsed Time (hh:mm)	Permeate Density (g/mL)	Slurry Temperature (°C)	Average Permeate Flow Rate (mL/min)
Batch 1	23:49	1.312	24.2	2.56
Batch 2	14:24	1.313	24.0	2.54
Batch 3	10:06	1.314	24.8	2.59

A useful comparison is to show the differential pressure increase for batch 2 as a function of either (i) the time from the start of the batch or (ii) the time from the previous backpulse. This information is provided in Figure 4.4. These data indicate that filter fouling occurred at an accelerated rate after the first backpulse. This result is to be anticipated, as the rate of fouling is generally seen to increase following each successive backpulse, see Geeting et al. (2018a, 2018b). As there are only two data points, it is not possible to extrapolate meaningfully how this rate of decline in performance will progress over a longer period of time.
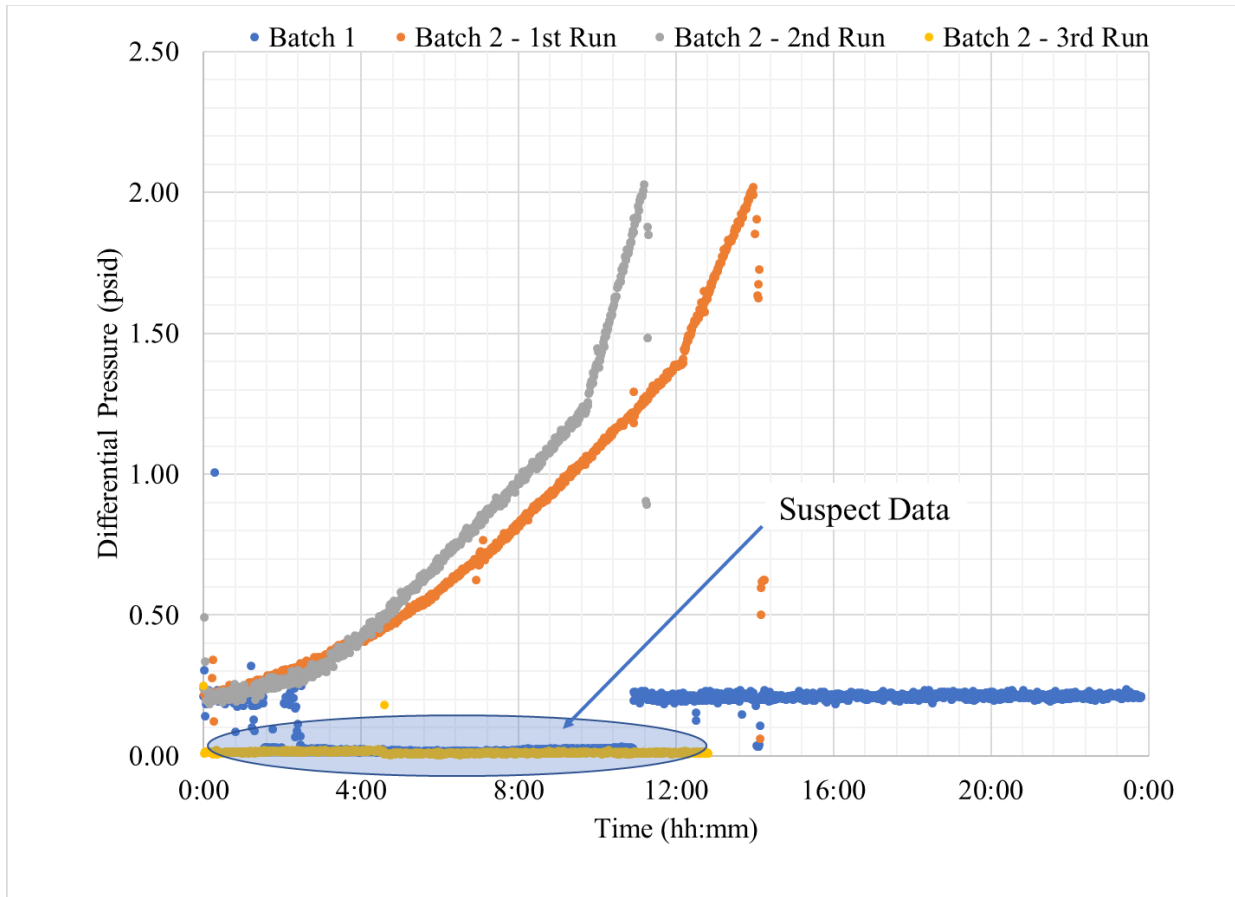
Figure 4.4. Filtration data stacked to compare fouling rate

It is also useful to assess the nature of the fouling that is occurring. Hermia (1982) describes four distinct fouling mechanisms, illustrated in Figure 4.5. Figure 4.6 shows a fit for three of those fouling mechanisms (intermediate blocking, complete blocking, and standard blocking) to the resistance as a function of volume produced. Note that the fourth mechanism, cake filtration, produced a linear fit when the resistance was plotted against the volume filtered. As there is clearly curvature in the data plotted in Figure 4.6, a fit for cake filtration was not included. Note that the resistance is calculated using a measured viscosity of 5 cP from the previous AP-105 filtration testing (Geeting 2018b). Inspection of Figure 4.6 indicates that intermediate blocking provides the best fit for the data.
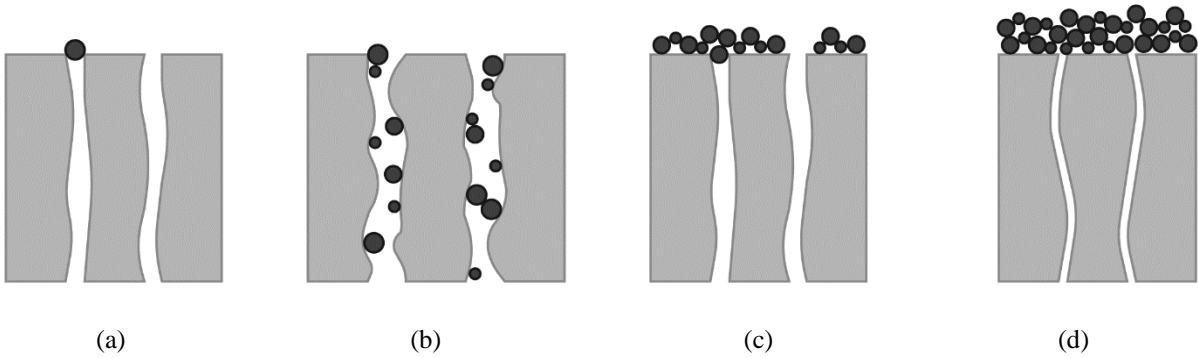
Figure 4.5. Filter fouling mechanisms: (a) complete blocking; (b) standard blocking; (c) intermediate blocking; (d) cake filtration
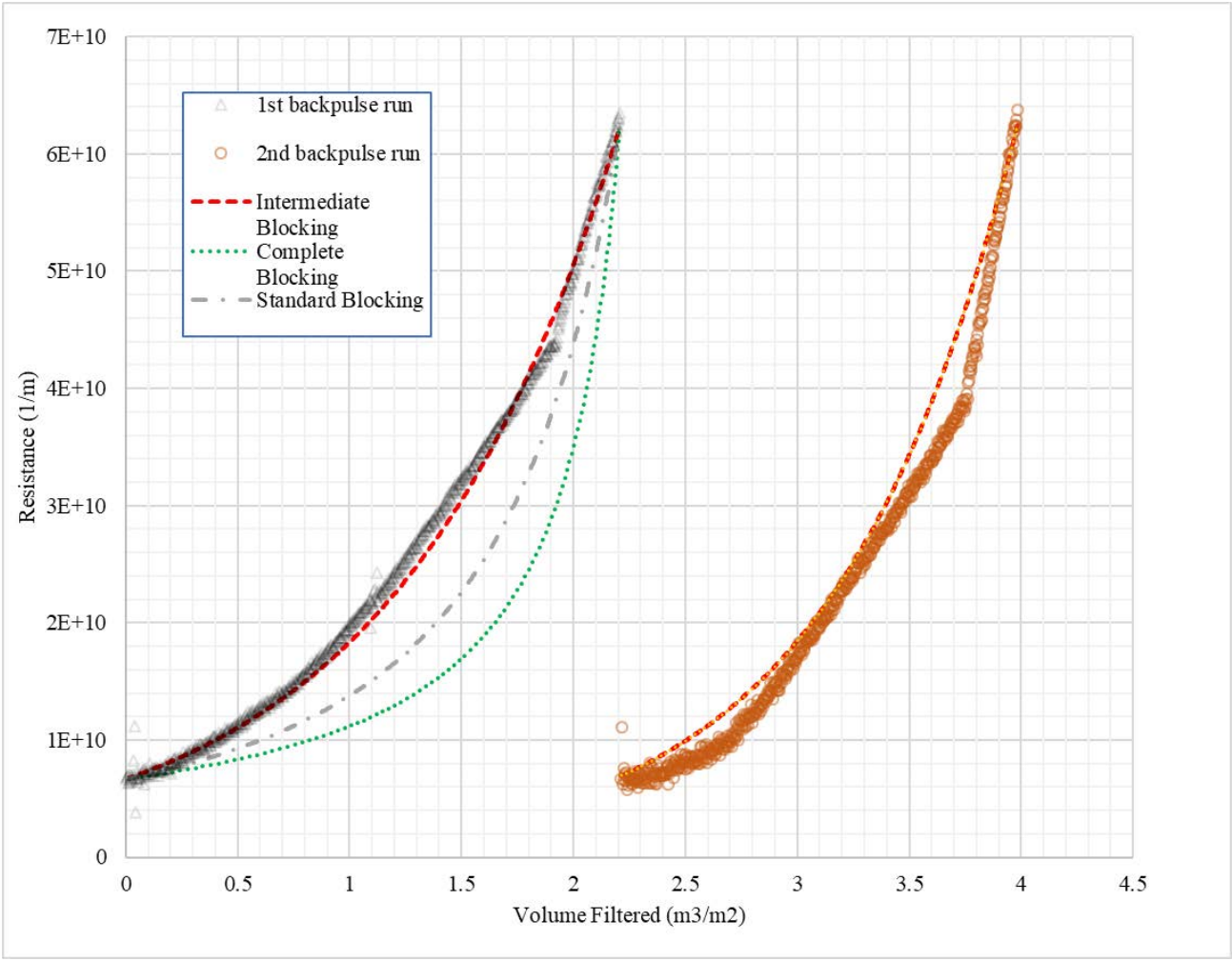
Figure 4.6. Fit to experimental data using classical fouling mechanisms

The fit results suggest that intermediate blocking is the mechanism that most closely represents the test data. Here, filter pores are fouled, and once fouled, additional solids can build up on the fouled surface. The following volumetric flow rate equations were derived from Hermia (1982):

$$Q(t) = Q_0 \, e^{-K_i V(t)}$$ Intermediate Blocking

$$Q(t) = Q_0 + K_b V(t)$$ Complete Pore Blocking

$$Q(t) = Q_0 \left(1 + \frac{K_s V(t)}{2} \right)^2$$ Standard (constriction) Blocking

where Q is the volumetric flow rate at time t, Q_0 is the initial volumetric flow rate, K_i is the intermediate blocking parameter, K_b is the complete blocking parameter, K_s is the standard blocking parameter, and $V(t)$ is the filtrate volume at time t. Curve fits were developed using the last data point before a backpulse. Table 4.4 details the blocking parameters used to fit the experimental data.

Table 4.4. Filter fouling curve fit parameters

	First Backpulse Run	Second Backpulse Run
$Q_0 \; [\frac{m^3}{m^2}]$	4.30×10^{-5}	4.60×10^{-5}
Intermediate blocking parameter; K_i, $[m^3]$	1.013	1.240
Complete blocking parameter; K_b, $[m^3]$	1.74×10^{-5}	--
Standard blocking parameter; K_s, $[m^3]$	0.610	--

Note that when a 0.1-micron filter is used (Geeting 2018b), the filter flux behaves as cake filtration. This suggests that for the 5-micron filter, there is some penetration of the solids into the pores of the filter, causing plugging of those pores. The decrease in time between required backpulses (i.e., the faster rise in transmembrane pressure) may be associated with a failure to dislodge some of those particles from the pores of the filter.

Darcy's law relates the flow rate through a porous media to the pressure drop causing that flow:

$$J(t) = \frac{\Delta P}{(\mu * R_{tot}(t))}$$

where J is the filter flux, ΔP is the transmembrane pressure, μ is the fluid viscosity, and R_{tot} is the total filtration resistance.

Rearranging produces:

$$R_{tot}(t) = \frac{\Delta P}{(\mu * J(t))}$$

Figure 4.7 shows the total filter resistance as a function of volume filtered over the 3 days of testing. Filter resistance increased from ~5.6×10^9 m^{-1} exponentially once batch 2 bottles were added to the slurry reservoir. Batch 2 reached filter resistance peaks outlined in Table 4.5 prior to backpulsing.

Table 4.5. Batch 2 test parameters prior to backpulsing

Test Event	Filtration Resistance (1/m)	Volume Filtered (m³/m²)	Transmembrane Pressure (psid)
Backpulse 1	6.31×10^{10}	2.204	2.02
Backpulse 2	6.37×10^{10}	1.773	2.03
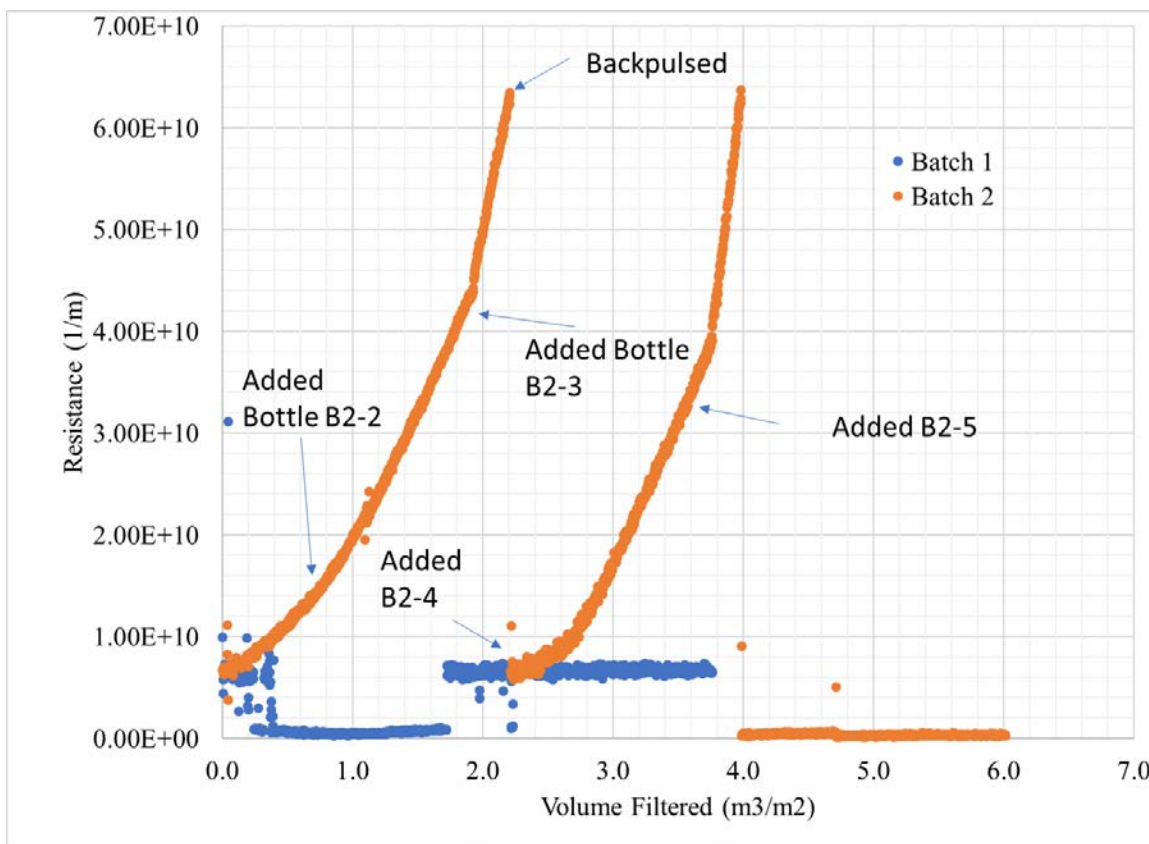
Figure 4.7. Batch 1 and Batch 2 BDEF filtration

4.3 Analytical Results

Process Water (River Water) Analysis

ICP-OES and IC analyses for the river water are provided in Table 4.6 on a mass-per-unit-volume basis (µg/mL). Some analyte results are shown in brackets; this indicates that the analytical result was less than the estimated quantitation limit (EQL) but greater than or equal to the method detection limit (MDL) and the associated analytical uncertainty could be higher than ±15%. The fractionation result was placed in brackets where it was calculated with one or more bracketed analytical values to highlight the higher uncertainty. The top five components measured in the river water were Ca, Si, Na, Mg, and S. There was no detectable F, NO_2, or NO_3 but the sample contained approximately 12 ppm SO_4 and 1 ppm Cl.

Table 4.6 Analyte Concentration in River Water (ASR 1074)

Analysis Method	Analyte	River Water (µg/mL)
	Ca	22.75
	Mg	4.88
	Na	2.43
	Si	2.17
	K	0.86
	Se	[0.290]
	Sr	0.12
	Zn	0.08
	P	[0.042]
ICP-OES	Ba	0.03
	Te	[0.026]
	Ru	[0.014]
	Ce	[0.012]
	Fe	[0.012]
	B	[0.007]
	Mo	[0.007]
	Dy	[0.003]
	Ag	[0.003]
	V	[0.003]
	Mn	[0.002]
	F	--
	Cl	1.3
Ion Chromatography (IC)	NO$_2$	--
	SO$_4$	12.4
	NO$_3$	--

Bracketed results were less than the estimated quantitation limit but greater than or equal to the method detection limit and analytical uncertainty could be higher than ±15%.

"--" indicates the recovery could not be calculated.

BDEF permeate samples

Total alpha analysis (alpha energy analysis, AEA) was conducted on the three permeate samples to determine the transuranic (TRU) content of the filtered permeate. The analysis is shown in Table 4.7 and shows no gross breakthrough of TRU components that aren't already soluble between the three permeate samples taken. All samples remained below the 0.1 µCi/g threshold defining TRU waste.

Table 4.7 AEA for permeate samples

Analysis Method	Sample ID	(µCi/mL)
Total Alpha Analysis	Permeate Sample 1	2.45E-04
	Permeate Sample 2	2.69E-04
	Permeate Sample 3	5.53E-04

BDEF Backpulse Solids Analysis

The dried sample mass collected from the backpulse concentrate indicates that the total solids loading of the diluted (5.6 M Na) AP-105 waste has an upper bound of 44 parts per million.

Table 4.8 summarizes the backpulse solids radioisotope concentrations as analyzed by GEA and AEA. All sample results for target isotopes are reported in units of Bq/g with estimates of the total propagated uncertainty reported at the 1-sigma level. The predominant gamma activity was from ^{137}Cs, which is soluble and expected in all samples. ^{239}Pu was the only analyte below the detection limit for GEA but was detectable by AEA. ^{155}Eu and ^{242}Cm were detected in the solids but with a high uncertainty of ~40%. The predominate alpha activity was from ^{241}Am.

Table 4.8 Radioisotope results for dried and concentrated backpulsed solids, Bq/g ± 1-σ

Analysis Method	Analyte	Backpulse Solids (Bq/g)	
Gamma energy analysis (GEA)	Co-60	2.58E+01	± 12%
	Cs-137	2.86E+05	± 2%
	Eu-152	5.70E+01	± 12%
	Eu-154	1.35E+03	± 2%
	Eu-155	1.96E+02	± 40%
	Am-241	5.27E+03	± 9%
	Pu-239	< 5.92E+05	
Separations/ Alpha energy analysis (AEA)	Pu-238	6.01E+02	± 6%
	Pu-239+240	4.26E+03	± 2%
	Am-241	1.31E+04	± 10%
	Cm-242	3.85E+01	± 41%
	Cm-243+244	3.29E+02	± 13%

ICP-OES and TIC/TOC analyses for the backpulsed solids are provided in Table 4.9 on a mass-per-unit-mass basis (µg/g). The top three components measured in the backpulsed solids were Na, Cr, and Al, with Mg, Ni, and Ca being on the same order of magnitude as Cr and Al. The high Na concentration can be attributed to the entrained 5.6 M salt solution wash used to rinse the solids. The K concentration in the

solids appears to be an order of magnitude less than the as-received AP-105 concentration, which is expected after the solids were rinsed and is likely residual AP-105 that was not fully washed off. Relative to the K concentration, Cr, Al, and Mg are present at high levels compared to the supernate and are determined to be the main components of the solid sample.

The TIC results indicate carbonate there is a fraction of solids that are carbonate. TOC analysis confirmed a high organic content of 3.14 wt%. Lower than the 9.2 wt% seen in previous AP-105 filtration testing (Geeting 2018b).

Table 4.9 Inorganic Analyte Concentrations in Backpulse Solids

Analysis Method	Analyte	Backpulse Solids (µg/g)
ICP-OES	Na	2.44E+05
	Cr	8.50E+03
	Al	6.21E+03
	Mg	5.00E+03
	Ni	2.66E+03
	Si	1.70E+03
	Fe	1.02E+03
	Ca	1.01E+03
	S	8.00E+02
	Pb	4.61E+02
	K	4.37E+02
	Se	2.10E+02
	Cu	1.66E+02
	Ba	1.30E+02
	Zn	1.18E+02
	Cd	9.34E+01
	As	8.70E+01
	Nd	6.75E+01
	P	6.10E+01
Hot persulfate oxidation	Total organic C	31,436
	Total inorganic C	2,593

4.4 Microscopy Solids Analysis

The SEM analysis revealed large block-like particles that ranged in size up to 100s of micrometers. The contrast-free appearance of the particles suggested that they may have formed from evaporation rather than precipitation in solution (see Figure 4.8). SEM-EDS analysis of selected particles identified in Figure 4.9 showed that most of the large particles were dominated by Na (O was excluded from the analysis) as summarized in Table 4.10. However, there were some Al-Si phases within these larger particles and a suggestion of the presence of other heavy metals. EDS mapping was performed to understand the distribution of these other elements in the larger particles. The SEM images did display a texture in the block-like particles, indicating the presence of fibrous strands within particles. This morphology was observed in the STEM images that are discussed later. It is important to note, SEM results are presented

for illustrative purposes; they are provided "For Information Only" (FIO) and are not considered quantitatively robust.
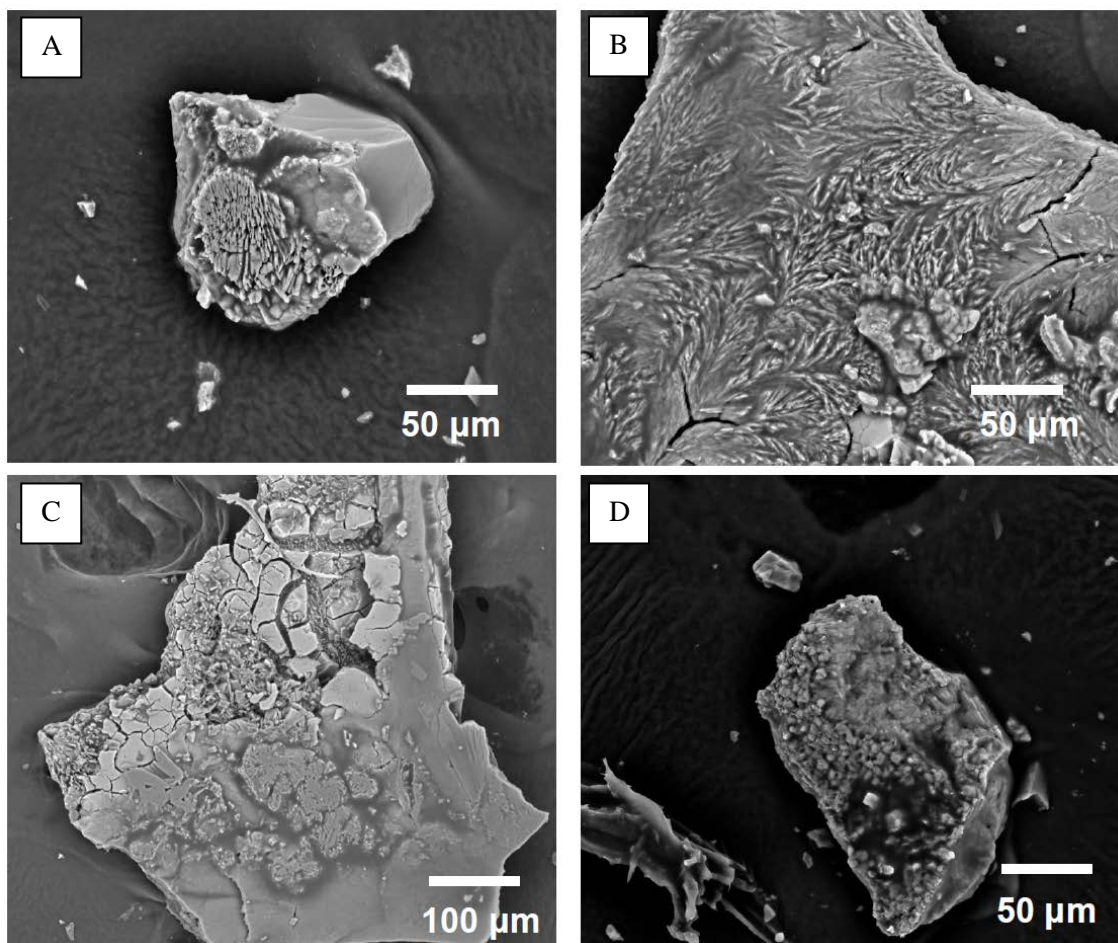
Figure 4.8. SEM images of large particles found in the backpulse concentrate, FIO

Table 4.10 Elemental analysis of selected particles in Figure 4.9 in atom %, FIO

Location	NaK	MgK	AlK	SiK	SK	KK	CaK	CsL	CrK	FeK	NiK
1	72.0	1.1	7.9	4.2	9.7	0.0	4.5	0.0	0.0	0.0	0.7
2	92.5	0.0	0.0	1.7	3.5	0.2	0.2	0.9	0.3	0.4	0.4
3	94.1	0.0	0.0	1.5	3.5	0.0	0.0	0.2	0.0	0.3	0.3
4	89.3	0.0	0.0	2.2	5.3	0.4	0.5	1.1	0.4	0.5	0.3
5	88.2	0.0	0.0	2.8	7.3	0.8	0.5	0.0	0.2	0.3	0.0
6	87.6	0.0	0.0	2.1	4.9	0.5	0.6	1.4	1.0	0.8	1.1
7	92.2	0.0	0.0	1.7	3.6	0.6	0.6	1.0	0.0	0.2	0.2
8	4.9	0.5	24.6	48.8	0.8	1.0	17.0	0.0	0.2	2.0	0.0
9	0.5	15.0	21.7	6.5	1.3	0.2	4.2	0.0	36.7	3.6	10.3
10	14.1	19.6	20.6	4.8	1.0	0.1	3.2	0.0	26.2	2.9	7.4
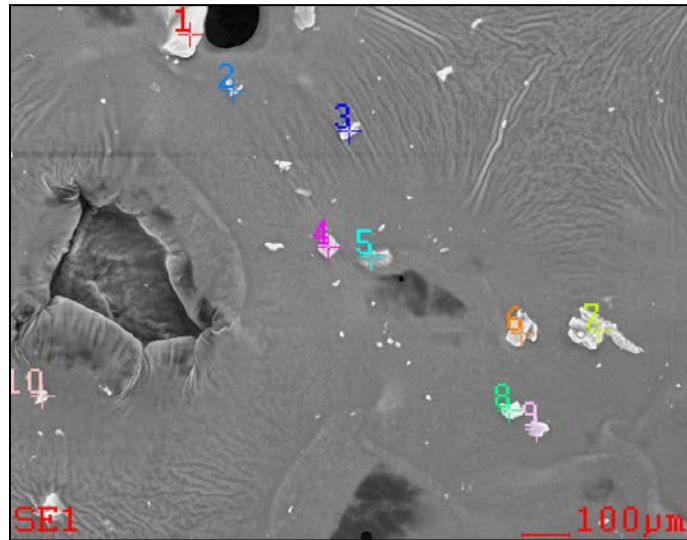
Figure 4.9. SEM image of the EDS analyzed particles found in the
backpulse concentrate that had a cake-like appearance, FIO
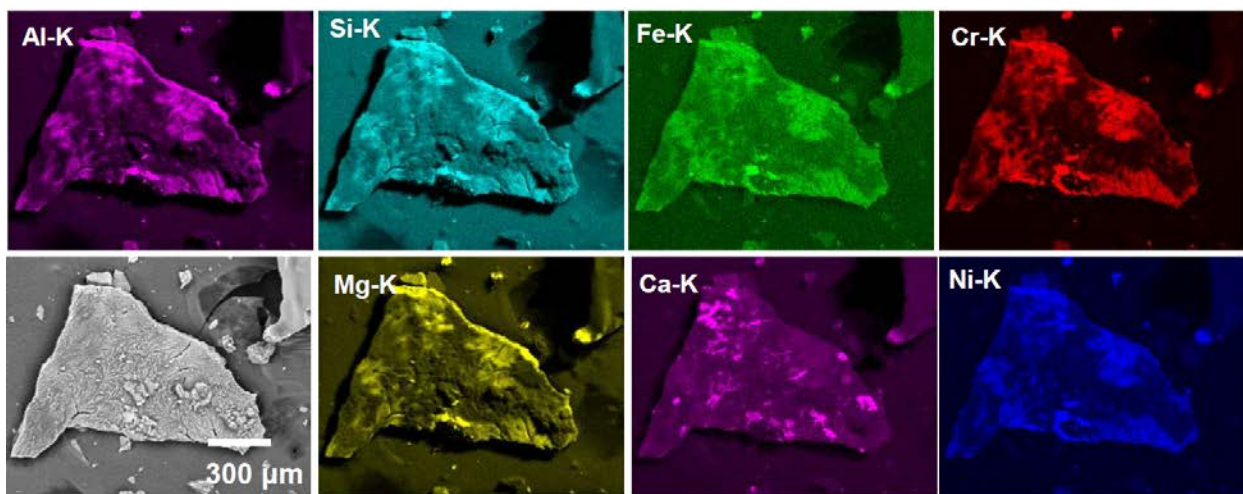
Figure 4.10. SEM-EDS elemental maps of the large particles found in the backpulse concentrate, FIO

The SEM elemental map (see Figure 4.10) revealed that these larger particles had regions enriched in Al, Si, and Ca, as well as Cr, Fe, and Ni. The particle size distribution was measured using a series of collected images. The image analysis reported the equivalent circular diameter of the particles as seen in Figure 4.11.
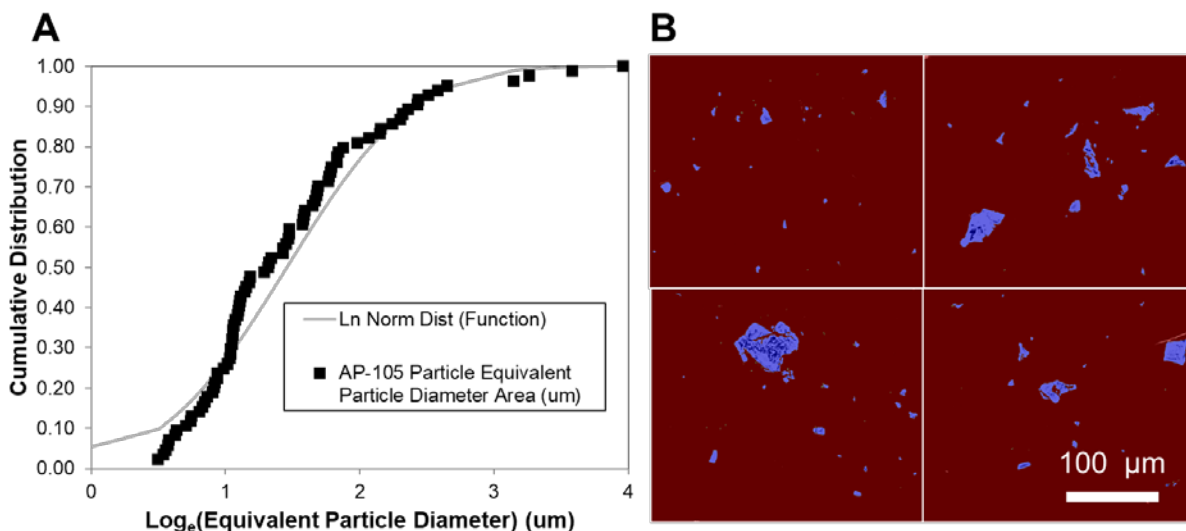
Figure 4.11. (A) Distribution of particles (equivalent circular diameter) in micrometers obtained from SEM images shown in (B) Image analysis software used to isolate particles (blue) for analysis from the background, FIO

The particle size distribution was fitted to a log-normal curve. The average particle diameter was determined to be 4.2 µm. The very large particles, in excess of 50 um in diameter, were dominated by sodium and likely salt particles. As described earlier, even larger salt particles were observed, for instance B in Figure 4.8; however, these were excluded from this analysis.

STEM analysis was used to understand the nature of the non-sodium-bearing salt precipitates in the specimen. The STEM images and elemental maps (see Figure 4.12, Figure 4.13, and Figure 4.14) highlighted the high-Z elements in the particles. The high-Z material was scattered heterogeneously through the particle agglomerates; however, the high-Z particles had agglomerated together to form larger particles.

Excluding the dominant sodium nitrate material from the solids washing process, there appear to be Al-silicates, mixed Cr-Al oxide, and Fe-oxides phases. Within these phases, localized enrichment of Mg and Ca was only partly visible. These compositions could be consistent with phases previously identified in tank wastes, such as cancrinite and Fe-oxides. STEM-EDS and electron diffraction was used to investigate whether these phases could be present in the sample.

In Figure 4.12, Al and Si are associated according to the elemental analysis but the larger particle observed was a pure Al-oxide phase. There was also a calcium particle (possibly calcite) and nano-sized particles of iron oxide. These particles had collected to form a larger agglomerate. These phases were mostly amorphous and were devoid of any well-defined morphology. Elemental analyses of different regions in the field of view shown in Figure 4.12 are listed in Table 4.11. The elemental maps reflect the net-counts of the elements and are not quantitative.
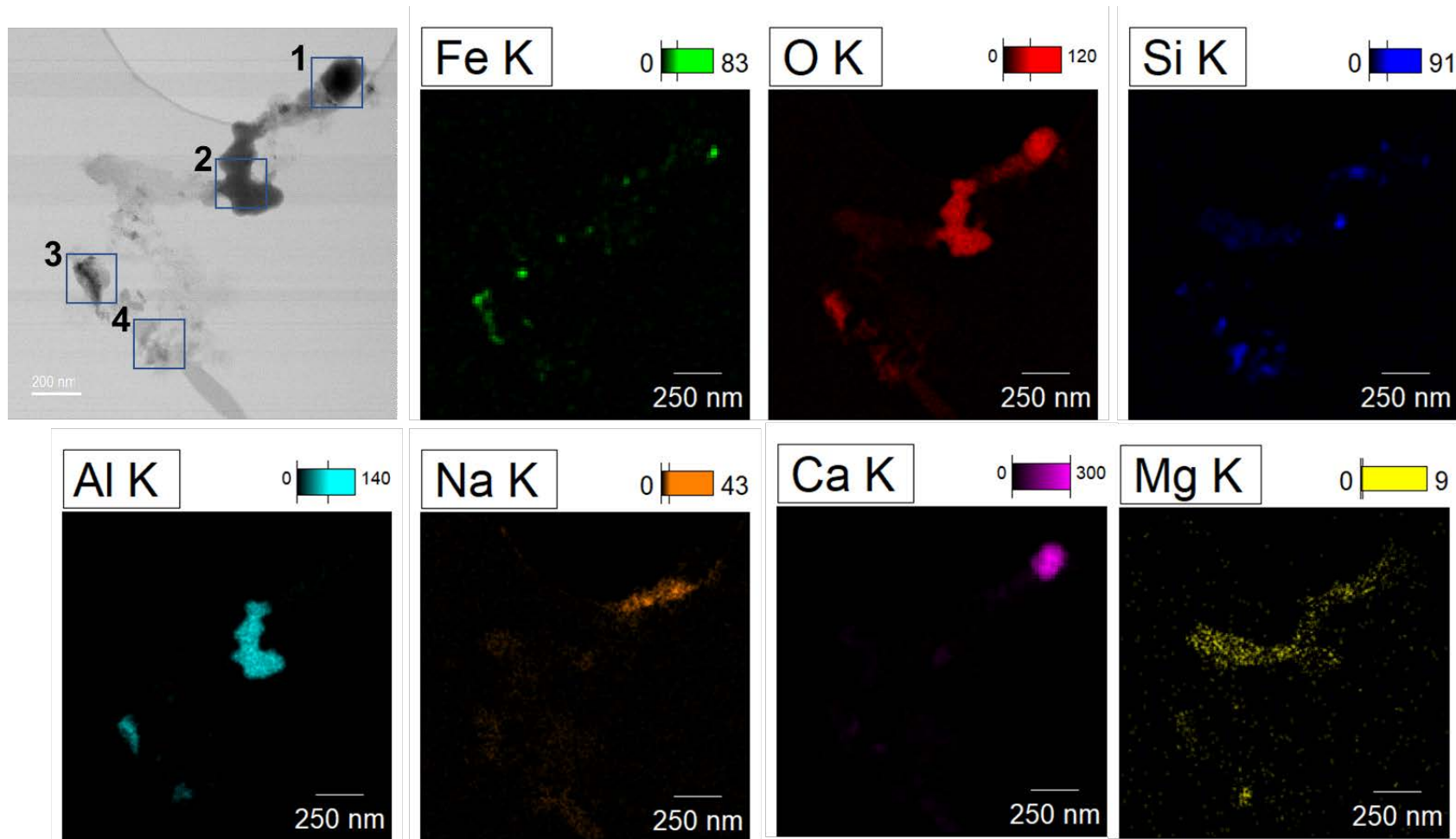
Figure 4.12. STEM image of particle agglomerate and EDS maps of the material showing the occurrence of Al-oxide and discrete Ca, Fe oxide, and Si particles, FIO

Table 4.11 Elemental analysis of Al-rich regions from Figure 4.12, FIO

Element	Region 1			Region 2			Region 3			Region 4		
	Net Counts	Weight %	Atom %	Net Counts	Weight %	Atom %	Net Counts	Weight %	Atom %	Net Counts	Weight %	Atom %
Na K	57	18.468	28.072	0	0	0	183	13.656	16.12	135	18.654	21.978
Al K	0	0	0	5311	99	99.325	1451	78.005	78.456	278	31.146	31.267
Si K	46	5.553	6.909	0	0	0	0	0	0	255	45.08	43.475
Ca K	3096	70.989	61.896	37	1	0.675	229	7.176	4.858	65	4.173	2.82
Fe K	127	4.991	3.123	0	0	0	114	1.163	0.565	49	0.948	0.46

Analysis of the Al-phase indicated that it was entirely Al oxide with little association with other elements. Both Na and S dominated all areas of the specimen. The composition observed in Region 3 had both Al and Si as well as Ca and is consistent with a zeolite-type phase. There were Fe-oxides but these were extremely small, on the colloidal size range. Similar analyses of other regions were obtained to develop an understanding of the different phase types and their distributions.
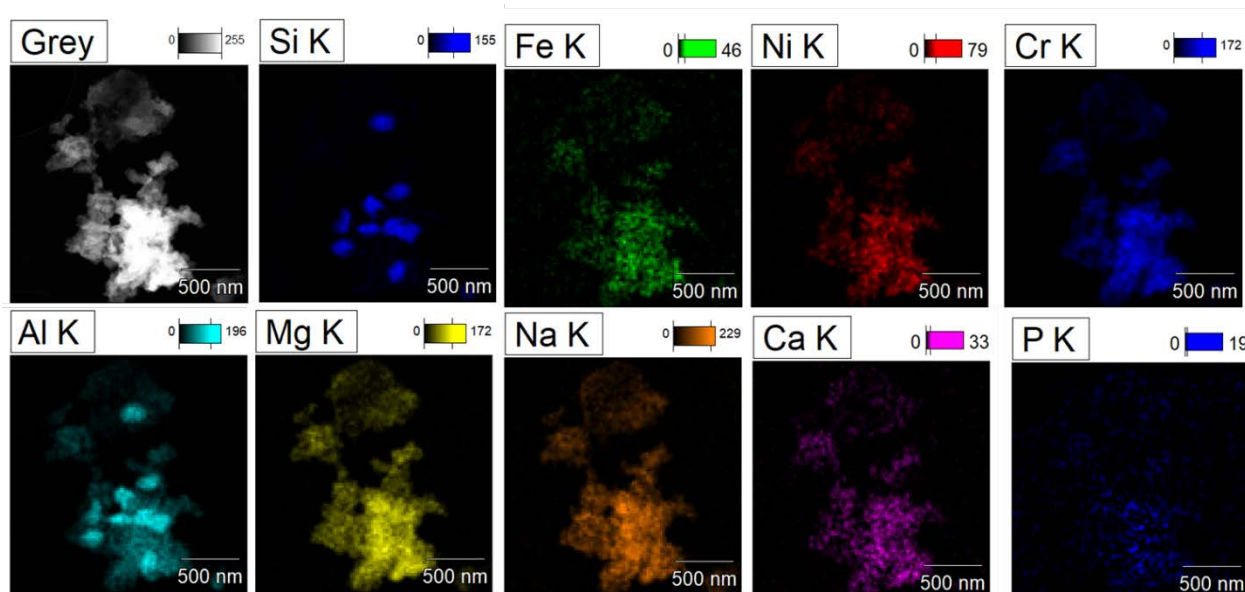
Figure 4.13. High-angle annular dark-field imaging (HAADF) image and STEM-EDS Analysis of a particle agglomerate showing a Si-Al phase as well as Cr phases, FIO

In Figure 4.13, Al again was present in a both a Si phase and in a phase containing various metals, including Cr and Mg. Even at these high magnifications, the phases seemed ill-defined. Electron diffraction of different phases was obtained (see Table 4.12); however, only a few single-crystal patterns were obtained, as much of the material was amorphous. X-ray diffraction (XRD) could be used to further probe these solids but this would require more material and XRD does not provide compositional analysis of the solids and would perform poorly with such small particles. Based on analysis of the electron diffraction (see Table 4.12) and the EDS results, there was good evidence of various Na-phases, including nitratite ($NaNO_3$), $NaNO_2$, NaOH, and $NaSO_4$. These Na-containing phases might have formed as evaporates. The second major type of particle were amorphous or semi-amorphous and contained heavier elements, including Al. The third type of phase was extremely small, colloidal, and may have existed in the supernatant prior to processing. These particles consisted of Fe, Cr, and other metals.

Table 4.12 Electron diffraction analysis of the particles, FIO

Al-Si particle, d/nm	Multiple phases, d/nm	Literature Values, d/nm	Reported Tank Waste Phases
	0.5616		
0.5086	0.4948	0.51933	$NaSO_4$
	0.46	0.48356	gibbsite
0.3879	0.4124		
	0.3317		
	0.3281		
	0.3031	0.30293	NaOH, nitratite
	0.28	0.29679, 0.297	NaOH, $NaNO_2$, cancrinite
0.2749		0.28164	nitratite
	0.2716	0.2786, 0.2731, 0.2608	$NaNO_2$, cancrinite
0.2323	0.2312	0.23025, 0.240, 0.2319	nitratite, cancrinite
	0.2206	0.22066	hematite
	0.2071	0.20324, 0.2034	$NaNO_2$, gibbsite
0.194	0.199	0.20041	NaAlOx
		0.19199	nitratite
	0.1891	0.18806	NaOH
	0.1835		
0.1747	0.1646	0.17831, 0.1693	NaAlOx, hematite
	0.1552	0.157	cancrinite
	0.1513		
0.1498	0.1472	0.1447, 0.1486	cancrinite, hematite
0.1393	0.1364	0.1364	cancrinite
0.1242	0.1257		
0.1184			
0.113			
0.1111			
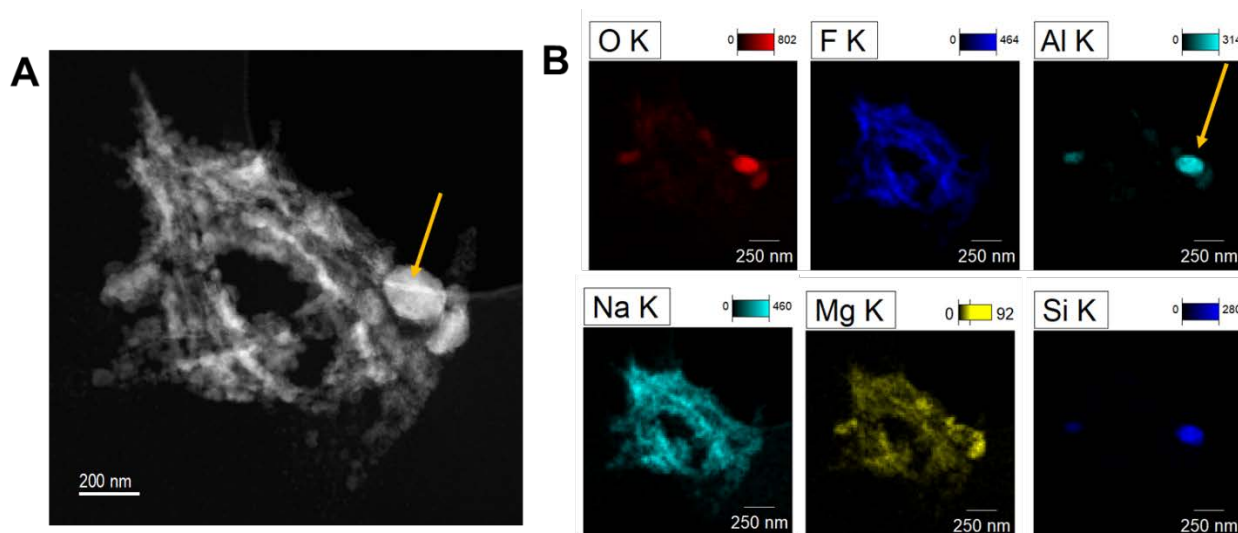
Figure 4.14. STEM image and EDS analysis of a particle agglomerate showing a Si-Al phase (see arrow) attached to salt-like phases, FIO

Figure 4.14 showed an Al-Si phase. The elemental map appeared to show no Ca in the phase and quantitative analysis suggested $MgAl_2SiO_6$. Most of the non-sodium salt particles in the sample were illusive and the results did not provide a definitive answer for the phases formed. The solids may have formed relatively rapidly but there is evidence that these particles have quickly bound together to form larger agglomerates. The Al-phase was not crystalline but may have formed rapidly during the dilution process. This could be investigated separately by characterizing the materials following this process. The smaller iron oxide particles that were identified in the elemental maps might be colloidal materials that existed prior to processing. Improved results could be obtained by dissolving the dominant Na-phases and re-analyzing the other particles with STEM. A second important observation from STEM images was the fibrous nature of the Na-dominated phase. This morphology was observed in the low-magnification SEM images and may reflect the formation mechanism for this material. There was close association of the Na-containing phases and the other particle types. Three groups of particles from the backpulse concentrate were identified from this microscopy analysis: (1) soluble Na-salts that formed large block-like particles but were made up of fibrous materials, (2) amorphous Al-phases, and (3) colloidal iron oxides.

5.0 Conclusions

The primary objective of this set of tests was to assess the impact of raw water dilution of Hanford tank waste supernate on the propensity to form solids and the filter performance with those solids. The results from this work are consistent with prior work that indicated that the addition of raw water results in solids formation. However, the quantity of solids formed was relatively small, on the order to 40 to 50 ppm. Even though the quantity of solids formed was small, the solids still adversely impacted BDEF filter operations performed here, requiring two backpulses to maintain operating conditions below the 2-psid TSCR threshold over the course of 72 test hours (11.4 m^3/m^2 specific volume filtered). In a bounding assessment, the reaction was complete within 6 months. The results from this work suggest that the reaction was likely complete by at most 3 months. Additional simulant testing (Daniel 2020) indicates that ~80% of all solids precipitated by dilution will be formed within the 3-month period following dilutions. Note that temperature changes can significantly impact to amount of solids that will form. This will be addressed through additional testing at lower temperatures in FY21.

Testing also demonstrated that settle/decant was effective at segregating the solids under the conditions tested. The sample that was allowed to sit quiescent for 6 months demonstrated a constant filter flux, indicating effectively no filter fouling. However, resuspension of the solids resulted in measurable increases in filter flux that required a backpulse frequency of 10 to 12 hours to return the filter to unfouled performance. The fouling observed is consistent with an intermediate fouling mechanism Hermia (1982), wherein individual pores are fouled concomitant with buildup of material on the surface of the filter. Note that the period between backpulses would likely decrease with successive backpulses, but the extent of change cannot be extrapolated based on the limited testing to date.

The required settling time in waste tank AP-105 or AP-107 cannot be assessed based on this set of tests. The conditions under which these samples were settled vary significantly from those present in high-level waste tanks. Work in FY21 will attempt to assess the degree of clarification that has been achieved to date at the pump suction.

6.0 References

ASME. 2000. *Quality Assurance Requirements for Nuclear Facility Applications*. NQA-1-2000, The American Society of Mechanical Engineers, New York, New York.

ASME. 2008. *Quality Assurance Requirements for Nuclear Facility Applications*. NQA-1-2008, The American Society of Mechanical Engineers, New York, New York.

ASME. 2009. *Addenda to ASME NQA-1-2008*. NQA-1a-2009, The American Society of Mechanical Engineers, New York, New York.

Daniel RC, CA Burns, RA Peterson, VL Saldana, and NL Canfield. 2020. *Testing of an AP-105 Precipitation Simulant.* PNNL-29690, Rev. 0 (RPT-DFTP-016, Rev. 0). Pacific Northwest National Laboratory, Richland, Washington.

Geeting JGH, JR Allred, AM Rovira, and RA Peterson. 2019. *Fiscal Year 2019 Filtration of Hanford Tank AP-107 Supernatant*. PNNL-28780, Rev. 0 (RPT-DFTP-015, Rev. 0). Pacific Northwest National Laboratory, Richland, Washington.

Geeting JGH, AM Rovira, JR Allred, RW Shimskey, CA Burns, and RA Peterson. 2018a. *Filtration of Hanford Tank AP-107 Supernatant*. PNNL-27638 (RPT-DFTP-009, Rev. 0). Pacific Northwest National Laboratory, Richland, Washington.

Geeting JGH, JR Allred, AM Rovira, RW Shimskey, CA Burns, and RA Peterson. 2018b. *Crossflow Filtration of Hanford Tank AP-105 Supernatant*. PNNL-27085 (RPT-DFTP-005, Rev. 0). Pacific Northwest National Laboratory, Richland, Washington.

Gerber MS. 1992. *Legend and Legacy: Fifty Years of Defense Production at the Hanford Site*. WHC-MR-0293, Rev. 2. Westinghouse Hanford Company, Richland, Washington. doi:10.2172/10144167

Hermia J. 1982. "Constant Pressure Blocking Filtration Laws – Application to Power-Law Non-Newtonian Fluids." *Transactions of the Institution of Chemical Engineers* 60(3):183-187.

Appendix A – BDEF Piping and Instrumentation Diagram
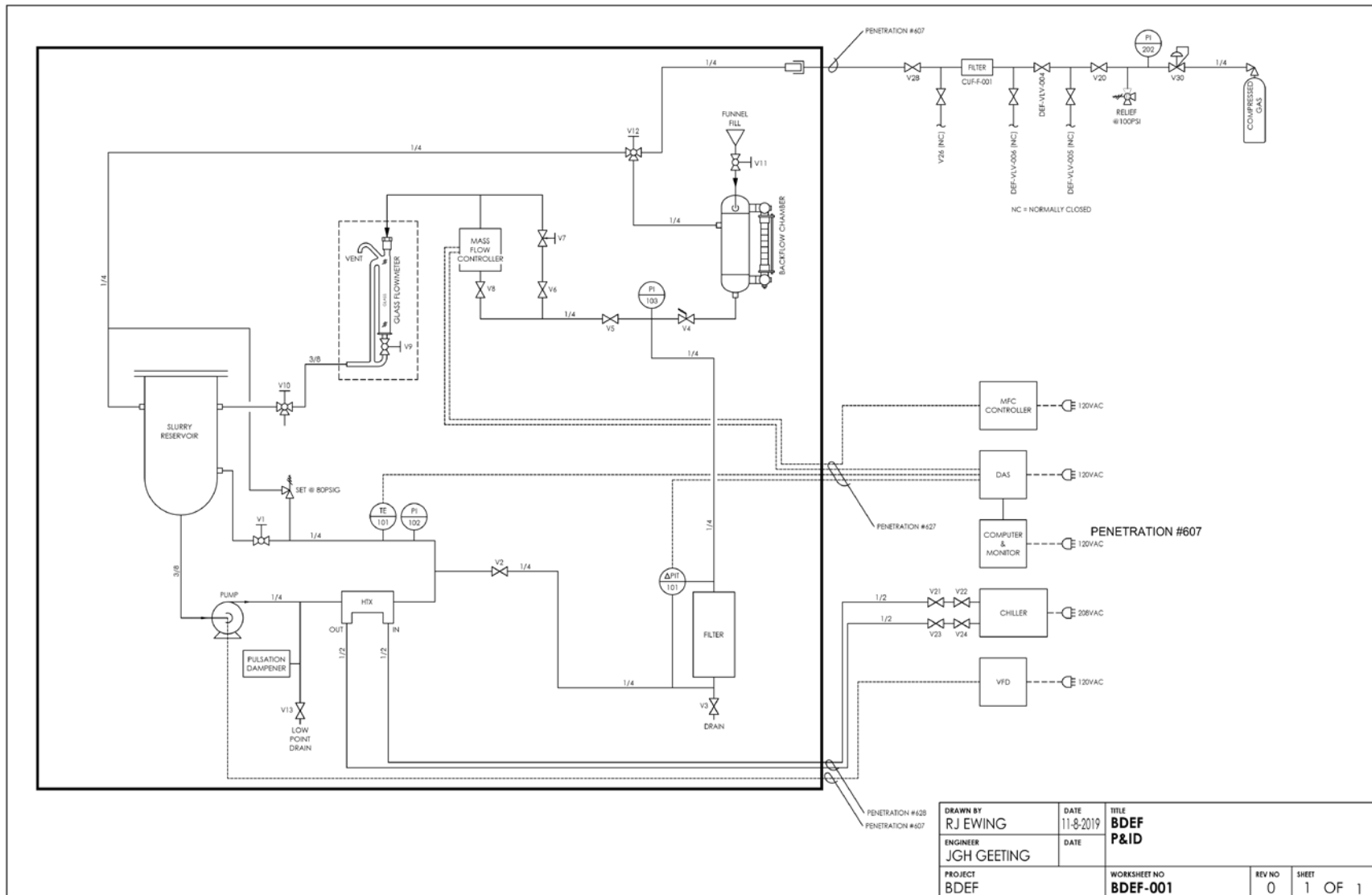
Appendix B – ICP-OES Results for Solid Observed in AP-105 Receipt Bottle

Battelle PNNL/RPL/Inorganic Analysis ... ICP-OES Analysis Report
PO Box 999, Richland, Washington 99352

Project / WP#: 75433 / NE4452
ASR#: 0961.00
Client: A. Rovira
Total Samples: 1 (solid)

ASO Sample ID	Client Sample ID	Client Sample Description	Sample Weight (g)
20-0346	AP-105 Solids	Solids in as-received AP-105 waste jars	0.0253

Sample Preparation: RPG-CMC-129, Rev. 0. "HNO3-HCl Acid Extraction of Solids Using a Dry-Block Heater", performed by L. Darnell on 01/14/20. Simple dilution of the dissolved sample in 5% v/v HNO3 performed by J. Carter on 01/14/20.

Procedure: RPG-CMC-211, Rev. 4, "Determination of Elemental Composition by Inductively Coupled Argon Plasma Optical Emission Spectrometry (ICP-OES)".

Analyst:	J. Carter	Analysis Date:	01/14/20	ICP File:	C0843

See Chemical Measurement Center 98620 file: ICP-325-405-3
(Calibration and Maintenance Records)

M&TE:				
☒	PerkinElmer 5300DV ICP-OES	SN: 077N5122002	RPL 405 Bench	
☒	Sartorius ME414S	SN: 21308482	RPL 420	
☒	Ohaus Pioneer PA224C	SN: B725287790	RPL 405 Bench	
☐	Mettler AT400 Balance	SN: 192720-92	RPL 405 FH #3	
☐	Mettler AT400 Balance	SN: 1113292667	RPL 420 FH #13	
☐	Sartorius R200D Balance	SN: 39080058	RPL 525 FH #9	

_____   1/15/2020
Report Preparer   Date

_____   01/16/2020
Review and Concurrence   Date

Page 1 of 1

Battelle PNNL/RPG/Inorganic Analysis ... ICPOES Data Report

		Run Date >	1/14/2020	1/14/2020	1/14/2020
		Process Factor >	1.0	1895.1	1895.1
			405 diluent	20-0346	
Instr. Det. Limit (IDL)	Est. Quant. Limit (EQL)	Client ID >	Lab Diluent	AP-105	
(µg/mL)	(µg/mL)	(Analyte)	(µg/mL)	(µg/g)	(µg/g)
0.0048	0.048	Al	[0.017]	9,180	9,370
0.0021	0.021	Cr	--	536	543
0.0017	0.017	Fe	[0.012]	570,000	583,000
0.0002	0.002	Mn	--	5,450	5,560
0.0072	0.072	Si	[0.011]	1,470	1,530
Other Analytes					
0.0021	0.021	Ag	--	--	--
0.0647	0.647	As	--	--	--
0.0048	0.048	B	[0.033]	2,230	2,360
0.0001	0.001	Ba	--	61.2	62.3
0.0001	0.001	Be	--	[1.0]	[1.1]
0.0215	0.215	Bi	--	[82]	[140]
0.0052	0.052	Ca	[0.0059]	820	818
0.0013	0.013	Cd	--	32.9	29.4
0.0082	0.082	Ce	[0.017]	--	--
0.0038	0.038	Co	--	[70]	[66]
0.0021	0.021	Cu	--	259	259
0.0023	0.023	Dy	--	--	--
0.0008	0.008	Eu	--	--	--
0.0134	0.134	K	--	330	360
0.0018	0.018	La	--	[13]	[6.9]
0.0014	0.014	Li	--	[6.1]	[8.3]
0.0017	0.017	Mg	--	[17]	[14]
0.0056	0.056	Mo	--	--	--
0.0072	0.072	Na	--	17,000	17,300
0.0114	0.114	Nd	--	--	[39]
0.0041	0.041	Ni	--	227	236
0.0371	0.371	P	--	[410]	[380]
0.0257	0.257	Pb	[0.033]	1,740	1,790
0.0050	0.050	Pd	[0.0059]	--	--
0.0143	0.143	Rh	--	[51]	--
0.0070	0.070	Ru	--	--	--
0.1089	1.089	S	--	--	[240]
0.0671	0.671	Sb	--	--	--
0.0987	0.987	Se	--	--	--
0.0267	0.267	Sn	--	[370]	[400]
0.0002	0.002	Sr	--	8.52	8.88
0.0331	0.331	Ta	--	--	[93]
0.0181	0.181	Te	[0.032]	[89]	[98]
0.0076	0.076	Th	--	--	--
0.0004	0.004	Ti	--	60.9	66.6
0.0291	0.291	Tl	[0.043]	[65]	--
0.0376	0.376	U	--	--	--
0.0012	0.012	V	[0.0014]	--	--
0.0128	0.128	W	--	[65]	[40]
0.0006	0.006	Y	--	--	--
0.0027	0.027	Zn	--	147	139
0.0013	0.013	Zr	[0.0031]	[20]	[20]

1) "--" indicates the value is < MDL. The method detection limit (MDL) = IDL times the "multiplier" near the top of each column. The estimated sample quantitation limit = EQL (in Column . times the "multiplier". Overall error for values ≥ EQL is estimated to be within ±15%.
2) Values in brackets [ ] are ≥ MDL but < EQL, with errors likely to exceed 15%.

ASR-0961 from C0843 Rovira Solids

Battelle PNNL/RPG/Inorganic Analysis ... ICPOES Data Report

QC Performance 1/14/2020

Criteria >	≤ 35%	80%-120%	80%-120%	≤ 10%
QC ID >	20-0346 Dup	LCS/BS	20-0346 + PS-A	20-0346 5-fold Serial Dil
Analytes	RPD (%)	%Rec	%Rec	%Diff
Al	2.0	99	102	0.9
Cr	1.3	96	99	0.3
Fe	2.3	96	95	3.5
Mn	2.0	98	99	0.8
Si	4.2	94	97	8.8
Other Analytes				
Ag		91	92	
As		102	101	
B	5.8	102	104	6.7
Ba	1.7	95	98	1.3
Be		98	98	
Bi		106	111	
Ca	0.2	98	101	6.8
Cd	11.5	95	99	
Ce		95		
Co		97	97	
Cu	0.2	99	100	2.3
Dy		95		
Eu		94		
K	8.7	95	98	
La		93		
Li		102	102	
Mg		97	99	
Mo		96	97	
Na	1.5	96	97	4.7
Nd		97		
Ni	4.2	97	99	
P		96	99	
Pb	2.8	98	98	
Pd		87		
Rh		92		
Ru		89		
S		89		
Sb		95	98	
Se		107	110	
Sn		94	95	
Sr	4.1	98	99	
Ta		97	99	
Te		94		
Th		93		
Ti	9.0	97	99	14.5
Tl		89	88	
U		99		
V		95	97	
W		99	100	
Y		97	99	
Zn	5.8	95	98	
Zr		97	100	

Shaded results are outside the acceptance criteria.
nr = spike concentration less than 25% of sample concentration. Matrix effects can be assessed from

ASR-0961 from C0843 Rovira Solids

Appendix C – Microscopy Sample Preparation and Methodology

Materials from the backpulse concentrate were examined with scanning electron microscopy (SEM) and with higher-resolution scanning transmission electron microscopy (STEM). For SEM analysis, a small quantity of the solid material was placed on a flat sticky carbon tape mounted on an aluminum stub using an applicator stick. The sample was then tested for loose particles by gently tapping the specimen on its side. The specimen was surveyed and checked for smearable activity. It was then examined using an FEI (Thermo-Fisher Inc., Hilsboro, OR) Quanta 250 Field Emission Gun (FEG) equipped with a backscattered electron (BSE) detector, transmission detector, and EDAX (EDAX Inc., NJ) Genesis x-ray energy dispersive spectroscopy (EDS) system in the RPL. No conductive carbon coat was used for sample preparation, so the instrument was operated in the low-vacuum mode. The analyses with SEM-EDS are reported as semi-quantitative. Images were analyzed with particle imaging software to determine particle size distributions.

Specimens were further examined with STEM using a JEOL (JEOL Inc., Japan) ARM300F (GrandARM) microscope equipped with annular dark field detectors, and X-ray EDS detectors. Diffraction patterns were calibrated with a NiO standard and were analyzed with Gatan (Gatan Inc., Pleasanton, CA) DigitalMicrograph™ 3.0 software.

Distribution List

Number of Copies		Number of Copies	
2	**Washington River Protection Solutions**	**6**	**Pacific Northwest National Laboratory**
	Kris Colosi		Jarrod Allred
	Matthew Landon		John Geeting
			Reid Peterson
			Amy Westesen
			Edgar Buck
			Information Release

* Copies will be distributed electronically

Pacific Northwest
National Laboratory

902 Battelle Boulevard
P.O. Box 999
Richland, WA 99354
1-888-375-PNNL (7665)

www.pnnl.gov